

Bifurcation Diagram of a Polydyne Cam with an Offset Flat-Faced Follower Mechanism

Louay S. Yousuf*

Department of Mechanical Engineering, San Diego State University, 5500 Campanile Drive, San Diego, California, 92182-1323, USA

ABSTRACT

A bifurcation diagram is used to measure how high the follower detaches from the cam profile due to follower offset. Bifurcation diagram has been investigated for distinct cam angular velocities and follower offsets. There is a clearance between the follower and its guides by taking into account the friction between the cam, follower, and the two guides. The impact between the cam, follower and the two guides is occurred due to the impulse and momentum phenomenon. The bifurcation diagram is examined the nonperiodic motion for the follower. The numerical simulation has been done using SolidWorks software. Follower movement is processed experimentally through an infrared 3-D camera device with a high precision optical sensor. Nonlinear dynamic of the follower is examined in the presence of follower offset. The contact point between the cam and the follower is considered in bifurcation diagram.

Keywords: Non periodic motion; Bifurcation diagram; Cam follower system; Nonlinear dynamics; Follower offset

NOMENCLATURE

O:	Follower offset, mm.
F.G.I.D. :	Follower guide's internal dimension, mm.
N	Angular velocity of the cam, rpm.
m:	Mass of the follower, Kg.
k:	Spring stiffness which locates at the end of the followerstem , N/mm.
c:	Viscous damping coefficient, N.s/mm.
k_t	Spring stiffness which locates between the follower andthe installation table, N/mm.
P_C	Contact force between the cam and the follower, N.
Φ :	Pressure angle, Degree.
Δ :	Preload extension, mm.
x, \dot{x}, \ddot{x} :	Linear displacement, velocity, and acceleration ofthe roller follower, mm, mm/s, mm/s ² .
V_c	Sliding Velocity of the follower stem due to impulsemomentum phenomenon, mm/s.
G:	Gravitational acceleration, mm/s ² .
h_1, h_2	Heights of position (1) and (2) respectively, mm.
C	Clearance between follower stem and its guide, mm.
R:	Radial distance from the origin point to the contact pointof the follower guide, mm.
θ :	Angle of the follower stem about z-axis, Degree.
F_C	Contact force between the follower stem and its guide,N.
B:	Half-width of contact zone, mm.
K_b	Contact bodies stiffness, N/mm.
d_1, d_2	Diameters of cylinder (cam) and flat surface (follower) respectively ($d_2 = \infty$), mm.
E_1, E_2	Elastic modulii of cylinder (cam) and flat surface (follower) respectively, N/mm ² .

Correspondence to: Louay S. Yousuf, Department of Mechanical Engineering, San Diego State University, 5500 Campanile Drive, San Diego, California, 92182-1323, USA, Tel: + 01521320909; E-mail: louaysabah1979@gmail.com

Received: April 13, 2021, **Accepted:** May 31, 2021, **Published:** June 07, 2021

Citation: Yousuf SL (2021) Bifurcation Diagram of a Polydyne Cam with an Offset Flat-Faced Follower Mechanism. J Appl Mech Eng .10:365.

Copyright: © 2021 Yousuf SL. This is an open access article distributed under the term of the Creative Commons Attribution License, which permits unrestricted use, distribution, and reproduction in any medium, provided the original author and source are credited.

ν_1, ν_2	Poisson's Ratios of the cylinder (cam) and the flatsurface (follower).
L:	Thickness for both cam and follower, mm.z Depth below the surface of contact, mm.
z:	Damping ratio.
Δ :	Penetration, mm.
E:	Equivalent modulus of elasticity, N/mm ² .
n:	Exponent.
μ_k :	Kinetic coefficient of friction.
$\mathbf{v}(x)_o, \mathbf{v}(x)_f$	Initial and final tangential velocities before and after impact respectively, mm/s.
$\mathbf{v}(y)_o, \mathbf{v}(y)_f$	Initial and final normal velocities before and after contact respectively, mm/s.
R_b :	Base circle radius of the cam, mm.
Ψ :	Angle of contact between the cam and the follower, Degree.
S(Ψ):	Horizontal movement of the contact point, mm.
S'(Ψ):	Vertical movement of the contact point, mm.
a:	Transformation angle for the Cartesian coordinates of the cam profile at the contact point, Degree.
x_c, y_c	Cartesian coordinates of the cam profile at the contact point, mm.
E:	Equilibrium Force exerted by the cam, N.

INTRODUCTION

Alzate et al. reported experimentally the occurrence of complex dynamical scenarios which includes a coexistence, discontinuity-induced bifurcations, and chaos. They noticed and detected the sudden transition to chaos due to the interruption of a complete chattering sequence [1]. Under the variation of the cam rotational speed, Alzate et al. observed that the follower is detached from the cam and showed an emergence of periodic impacting behavior [2]. Osorio et al. analyzed the bifurcation and chaos in piecewise smooth dynamical systems at high rotational speeds [3]. They explained the transition to chaos in the presence of nonautonomous impact oscillator of bifurcation analysis. Yang et al. showed that the cam and follower kept in permanent contact when the cam spinning at low speed while the separation is occurred at high speeds under the action of gravity [4,5]. They used Moreau time-stepping method to describe the oblique-impact equations of the bifurcation analysis at different angular speed of the cam. The solution of oblique-impact equations of the bifurcation analysis for cam-follower has been extended by Lu to control the nonlinear response of the follower [6]. They showed numerically that the cam-follower system performs very complex nonlinear characteristics, such as period, quasi-period and chaos responses. Moreover, Valencia built a bifurcation diagram under the variation of cam rotation speed in which the follower impact is occurred just at the discontinuity point of the cam [7]. They presented smooth and nonsmooth bifurcations of nonlinear analysis of a cam-follower impacting system using a cam with non-smooth profile. Yousuf found the bifurcation diagram of the follower position based on the angular displacement of the follower at different angular velocity for the cam [8]. The aim of this paper, is to study the effect of follower offset on the bifurcation diagram for different position of the follower.

EXPERIMENTAL METHOD

Data acquisition technique through a signal processing approach is used to measure follower linear movement in the presence of follower offset. Follower guide's internal dimension (F.G.I.D.=16 mm) with distinct angular velocity of the cam and follower offsets (O=20, 30, 40, 50 mm) is used in the experiment. A macro sensor through an infrared marker of OPTOTRAK/3020 is used to capture follower movement in the y-direction. The follower is

moved with three degrees of freedom by taking into consideration the effect of gravity in the vertical direction. The macro sensor is a linear variable differential transformer (LVDT) of a model number (DC750-5001) [9]. LVDT converts the analog signal of the follower motion to a digital signal in which it will be readable using an optical sensor. The optical sensor is located on the follower in which locates at (x:0, y: 158.05 mm, z: 0). The polydyne cam is installed on the shaft of the motor which rotates at uniform angular velocity. Figure 1 shows the experiment rig test of a polydyne cam with flat-faced follower in the presence of follower offset. Due to the interface feedback of an infrared 3-D camera of the OPTOTRAK/3020 device, the follower movement is stocked in an excel file. The follower displacement is processed using MatLab software [10].

Impact and contact parameters in the presence of follower offset

The following impact parameters have been entered to SolidWorks software in order to do the contact between the cam and the follower and between the follower and its guides. The follower linear displacement, velocity, and acceleration has been extracted

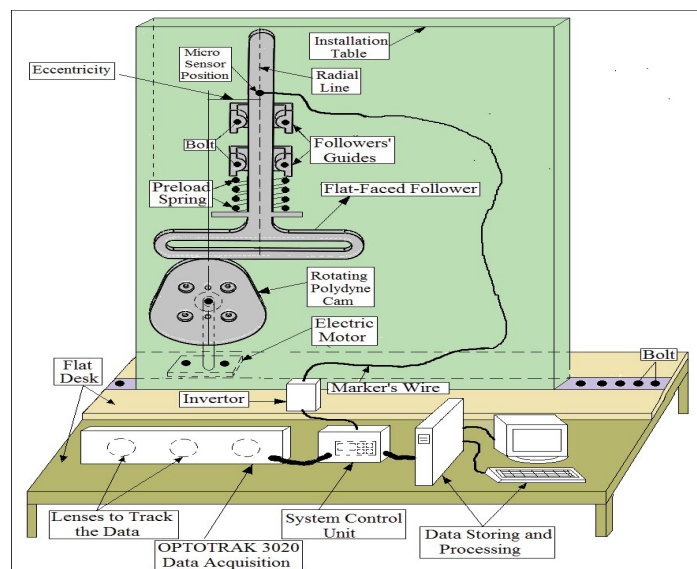


Figure 1: Cam-follower test rig in the presence of follower offset.

after inserting the list of parameters that mentioned below in SolidWorks software:

(a) The normal force between the cam and the follower is illustrated in the following equation [11]:

$$P_c = \frac{1}{\cos(\phi)} [k_1(\Delta + x(t)) - kx(t) - c\dot{x}(t) - m\ddot{x}(t)] \quad (1)$$

Where:

$$\phi = \tan^{-1}\left(\frac{x(t)+0}{x(t)+\sqrt{R_b^2+O^2}}\right), \quad (12)$$

(b) As mentioned in our previous publication that the velocity of contact is occurred due to impulse and momentum theory. When the follower starts spinning by an angle θ , the change in height has been happened from point (1) to point (2), as shown in Figure 2 and equation (2).

$$V_C = \sqrt{2g(h_1 - h_2)} \quad (2)$$

Where:

$$x = C$$

$$h_2 = \sqrt{R^2 - C^2}$$

$$\tan(\theta) = \frac{c}{h_2}$$

(c) The contact between the follower stem and the guides is considered as the contact between the flat surface and the cylinder [12,13]. From Figure 2 it can be concluded that the contact force between the follower stem and its guide is shown in the following equation, as in below:

$$F_C = [k_1(\Delta + x(t)) - kx(t) - c\dot{x}(t)] - m\ddot{x}(t)\sin(\theta) - mV_C\sin(\theta) \quad (3)$$

(d) The line of contact will become a rectangular contact zone of a half-width of Hertzian contact (b), as in below [13,14]:

$$b = K_b\sqrt{P_C} \quad (4)$$

Where:

$$K_b = \sqrt{\left(\frac{2}{\pi L}\right) \frac{(1-\nu_1^2/E_1 + (1-\nu_2^2)/E_2)}{(1/d_1) + (1/d_2)}} \quad (5)$$

(e) The depth (z) underneath the surface of contact in terms of damping ratio is as below [13]:

$$\zeta = \frac{z}{b} \quad (6)$$

The penetration distance (δ) is related to the field surface displacement and is characterized by Yousuf and Marghitu [13]:

$$\delta = 1.54 \left(\frac{2P_c^2}{2E^2d_1}\right)^{1/3} \quad (7)$$

Where:

$$\frac{1}{E} = \frac{1-\nu_1^2}{E_1} + \frac{1-\nu_2^2}{E_2}$$

(g) The flattening law of the shape predicts the value of the exponent (n) of the first asperity. The exponent value of (n) is ranging from (1.5) for (spherical punch) to (2) for (wedge shaped punch) [13-15].

(h) The effective kinetic coefficient of friction is calculated from the tangential and the normal velocities before and after the contact. The kinetic coefficient of friction is as in below [16].

$$\mu_k = \frac{m[v(y)_f - v(x)_o]}{m[v(y)_f - v(y)_f]} \quad (8)$$

Comparison of follower linear displacement in the presence of follower offset

In this paper, the cam profile with return-dwell-risedwell-return-dwell-rise-dwell is selected [17]. The follower displacement comparison is shown in Figure 3 for one cycle of cam rotation when the follower offsets to the left (O=10 mm) at (F.G.I.D.=0.5 mm) and (N=300 rpm).

Follower linear displacement is tracked experimentally using the optical sensor mounted on the follower through a 3-D lenses camera in the OPTOTRAK/3020 device. Solidworks software is used to simulate follower linear displacement numerically.

Bifurcation diagram in the presence of follower offset

The bifurcation diagram measures how high that the follower detaches or bounces from the cam at high speeds. At some high speeds, the follower will stay in contact with the cam based on the value of contact force. Bifurcation diagram is a tool to investigate the non-periodic motion of the follower based on the difference in angular displacement. In bifurcation diagram, when there will be a difference in angular displacement between the follower and the cam which means that the follower detaches from the cam (non-periodic motion for the follower). When the difference in angular speeds is zero which means that the follower stays in permanent contact with the cam (periodic motion for the follower). The point of contact between the cam and the follower is the reference point

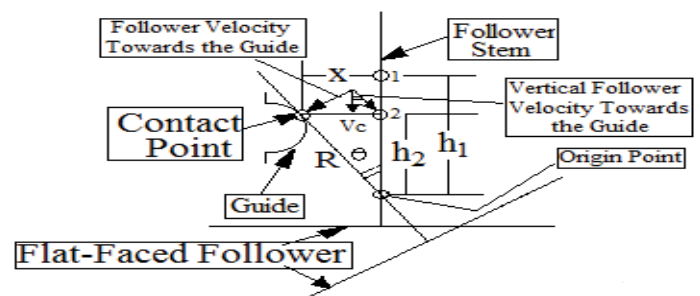


Figure 2: Contact model of flat-faced follower and its guide [8].

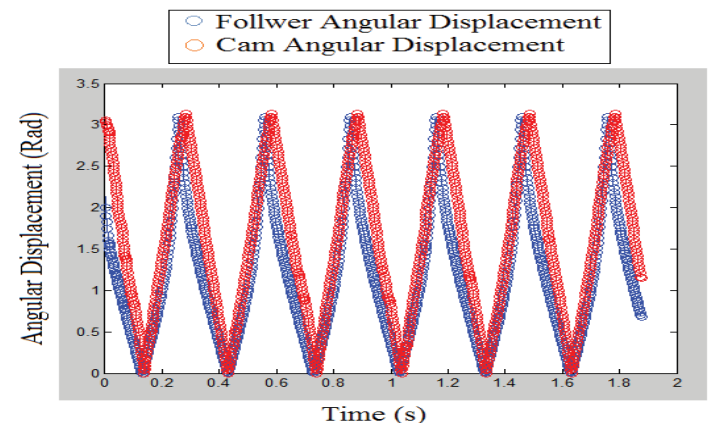


Figure 3: Comparison of follower linear displacement.

for measuring the bifurcation diagram [18]. Figure 4 shows how the cam and the follower stay in permanent contact when the angular displacement of the follower compatibles with the angular displacement of the cam at (F.G.I.D.=17 mm) and (N=300 rpm) when the follower offsets to the left (O=40 mm).

Cam profile verification in the presence of camshaft eccentricity

The Cartesian coordinates of cam profile along (x and y) directions have been started from the radius of the base circle of the cam as indicated in the following equation [18]:

$$x = S(\psi)\sin(\psi)+S'(\psi)\cos(\psi) \tag{9}$$

$$y = S(\psi)\cos(\psi)-S'(\psi)\sin(\psi) \tag{10}$$

Where:

$$S(\psi) = R_b + e \sin(\psi), \tag{18}$$

And,

$$S'(\psi) = e \cos(\psi), \tag{18}$$

The transformation of cam profile coordinates when the axis of rotation starts at the contact point is indicated in the matrix below:

$$\begin{bmatrix} x_c \\ y_c \end{bmatrix} = \begin{bmatrix} \cos(a) & \sin(a) \\ -\sin(a) & \cos(a) \end{bmatrix} \times \begin{bmatrix} x \\ y \end{bmatrix} \tag{11}$$

Substitute Eqn.(9) and Eqn.(10) into Eqn.(11), the equations that represent the cam profile in the presence of camshaft eccentricity are:

$$x_c = (R_b + e \sin(\psi))(\sin(\psi)\cos(a) + \cos(\psi)\sin(a)) + e \cos(\psi)(\cos(\psi)\cos(a) - \sin(\psi)\sin(a)) \tag{12}$$

$$y_c = (R_b + e \sin(\psi))(\sin(\psi)\cos(a) - \cos(\psi)\sin(a)) - e \cos(\psi)(\cos(\psi)\cos(a) + \sin(\psi)\sin(a)) \tag{13}$$

After simplification, the Cartesian coordinate equations at the point of contact in the presence of camshaft eccentricity are:

$$x_c = (R_b + e \sin(\psi))\sin(\psi+a) + e \cos(\psi) \cos(\psi+a) \tag{14}$$

$$x_y = (R_b + e \sin(\psi))\cos(\psi+a) + e \cos(\psi) \sin(\psi+a) \tag{15}$$

Figure 5 shows the comparison of polydyne cam profile in the presence of camshaft eccentricity. The numerical simulation of nonlinear dynamic response of the follower is carried out using SolidWorks software. The analytic solution of cam profile is done using Eqn.(14) and Eqn.(15).

RESULTS AND DISCUSSION

Figures 6 and 7 show the difference between the angular displacement of the follower and the angular displacement of the cam at distinct angular velocity for the cam. The systems with follower offset (O=40 mm) to the left and (O= 50 mm) to the right at (F.G.I.D.=17 mm) respectively are selected.

Figures 8 and 9 show the follower linear displacement against the time at distinct cam angular velocities. The systems with follower offset (O=40 mm) to the left and (O = 50 mm) to the right at (F.G.I.D.=17 mm) respectively are selected. The follower stays in permanent contact when the cam starts spinning at (N=200 rpm) and (N=400 rpm), while the follower starts detaching from the cam at (N=1000 rpm) as shown in Figure 8. The follower also starts jumping a little bit higher from the cam at (N=800 rpm) as shown in Figure 9.

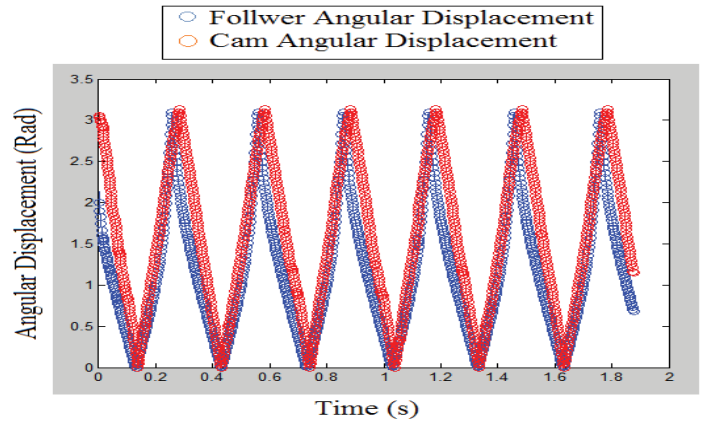


Figure 4: Angular displacement against time for the follower and the cam.

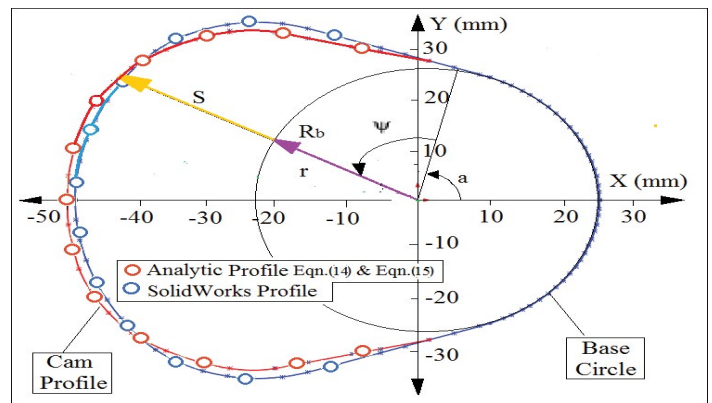


Figure 5: Comparison of cam profile in the presence of camshaft eccentricity.

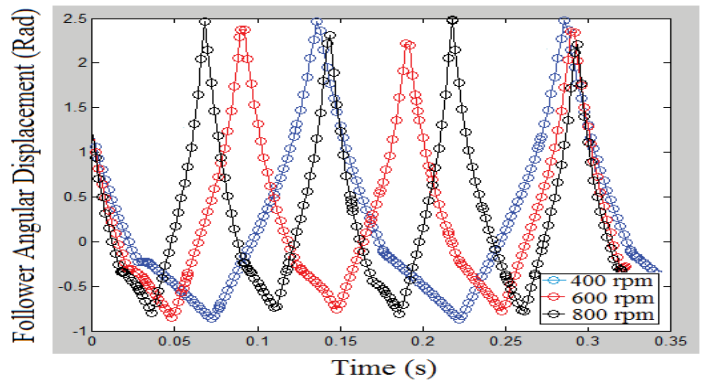


Figure 6: Difference in angular displacement of the follower and the cam at distinct angular velocities at follower offset (O = 40 mm).

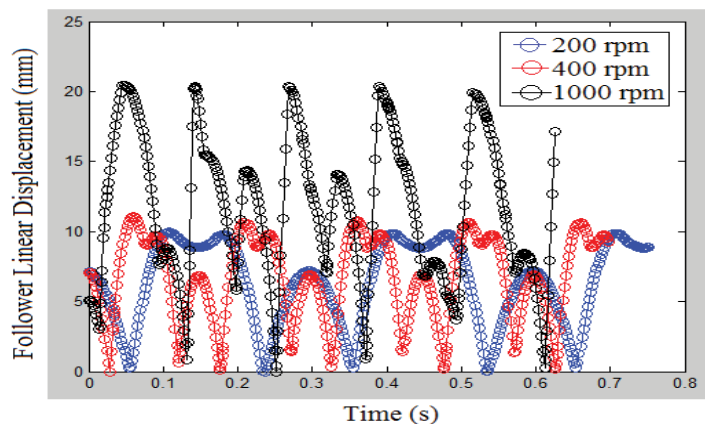


Figure 7: Difference in angular displacement of the follower and the cam at distinct angular velocities at follower offset (O = 50 mm).

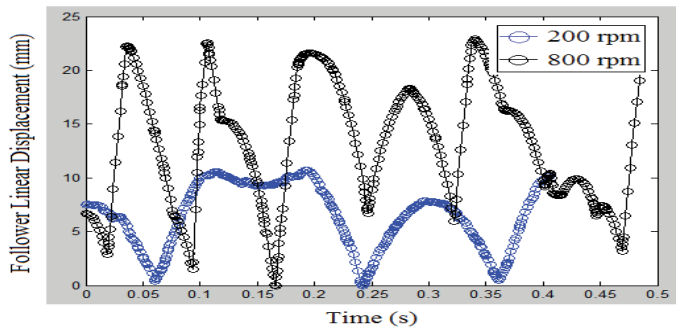


Figure 8: Follower linear displacement against the time at distinct cam angular velocities when the follower offsets to the left ($O = 40$ mm).

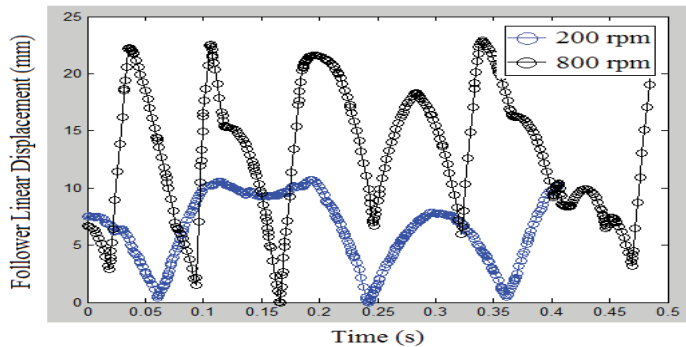


Figure 9: Follower linear displacement against the time at distinct cam angular velocities when the follower offsets to the right ($O = 50$ mm).

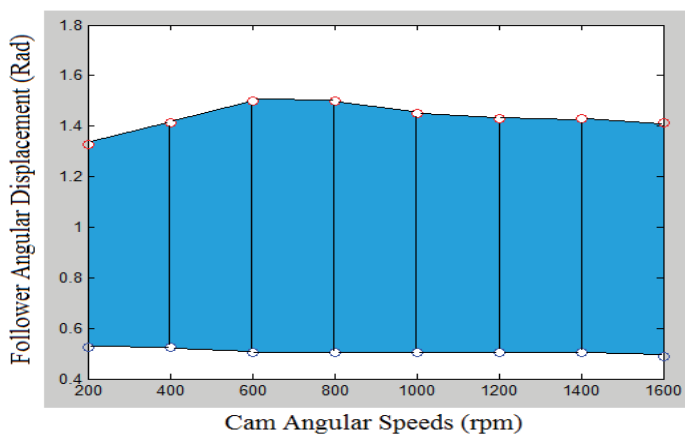


Figure 10: Bifurcation diagram of the follower angular displacement when the follower offsets to the left ($O = 40$ mm).

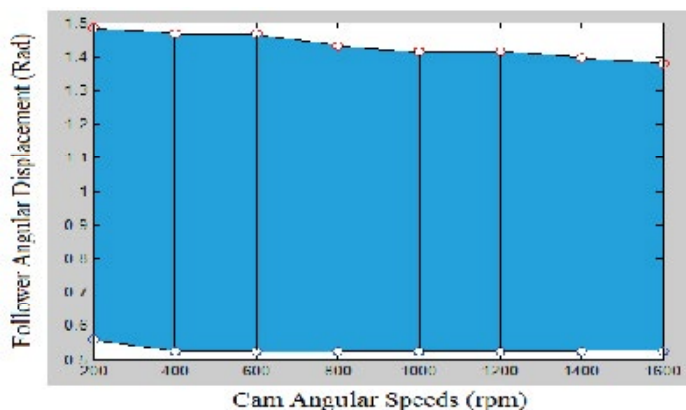


Figure 11: Bifurcation diagram of the follower angular displacement when the follower offsets to the right ($O = 50$ mm).

Figures 10 and 11 show the bifurcation diagram of follower angular displacement against cam angular velocities. The systems

with follower offset ($O=40$ mm) to the left and ($O=50$ mm) to the right at (F.G.I.D.=17 mm) respectively are selected. The non-periodic motion increased with the increasing of cam angular velocities since it reaches ($N=600$ rpm). After that the non-periodic motion decreases with the increasing of cam angular velocity until the nonperiodic motion settles down at ($N=1000$ rpm) as indicated in Figure 9. Moreover, the non-periodic motion decreased with the increasing of cam angular velocities in which settles down at ($N=800$ rpm) as illustrated in Figure 10.

CONCLUSION

According to bifurcation diagram that the non-periodic motion increased with the increasing of cam angular velocities since it reaches ($N=600$ rpm). After that the nonperiodic motion decreases with the increasing of cam angular velocities in which the non-periodic motion settles down at ($N=1000$ rpm) when the follower offsets to the left ($O=40$ mm) and at (F.G.ID.=17 mm). Moreover, the nonperiodic motion decreased with the increasing of cam angular velocities in which settles down at ($N=800$ rpm) when the follower offsets to the right ($O=50$ mm).

ACKNOWLEDGMENTS

I want to first thank the reviewers and the editor for re-viewing my paper.

REFERENCES

1. Alzate R, Di Bernardo M, Giordano G, Rea G, Santini S. Experimental and numerical investigation of coexistence, novel bifurcations, and chaos in a cam-follower system. *SIAM J Appl Dyn Syst.* 2009;8(2):592-623.
2. Alzate R, Di Bernardo M, Montanaro U, Santini S. Experimental and numerical verification of bifurcations and chaos in cam-follower impacting systems. *Nonlinear Dyn.* 2007;50(3):409-29.
3. Osorio G, di Bernardo M, Santini S. Corner-impact bifurcations: a novel class of discontinuity-induced bifurcations in cam-follower systems. *SIAM J Appl Dyn Syst.* 2008;7(1):18-38.
4. Yang YF, Lu Y, Jiang TD, Lu N. Modeling and nonlinear response of the cam-follower oblique-impact system. *Discrete Dyn Nat Soc.* 2016; 19:2016.
5. Alzate R, Piiroinen PT, Di Bernardo M. From complete to incomplete chattering: A novel route to chaos in impacting cam-follower systems. *Int J Bifurcat Chaos.* 2012;22(05):1250102.
6. Lu N, Ren XM, Jiang TD, Yang YF. Impulsive control of a cam-follower oblique-impact system. *J Mech.* 2018;34(4):475-482.
7. Valencia J, Osorio G. Nonlinear numerical analysis of a cam-follower impacting system. In: 2011 IEEE Second Latin American Symposium on Circuits and Systems (LASCAS), IEEE 2011;23:1-4.
8. Yousuf LS. Investigation of chaos in a polydyne cam with flat-faced follower mechanism. *J King Saud Univ Eng Sci.* 2020;9.
9. Yousuf LS, Marghitu DB. Analytic and numerical results of a disc cam bending with a roller follower. *SN Applied Sciences.* 2020;2(10):1-5.
10. Yousuf LS, Marghitu DB. Non-linear dynamics behavior of cam-follower system using concave curvatures profile. *Adv Mech Eng.* 2020;12(9):1687814020945920.
11. Shakoor MM. Fatigue life investigation for cams with translating roller-follower and translating flat-face follower systems.
12. Tsiafis, I, Mitsi, S, Bouzakis, K, Papadimitriou A. Optimal design

- of a cam mechanism with translating flat-face follower using genetic algorithm. *Tribol Ind.* 2013; 35(4):255-260.
13. Yousuf LS, Marghitu DB. Non-linear dynamic analysis of a cam with flat-faced follower linkage mechanism. In: *ASME International Mechanical Engineering Congress and Exposition*. American Society of Mechanical Engineers. 2017; 3 (58370): V04AT05A051.
 14. Shigley JE. *Shigley's mechanical engineering design*. Tata McGraw-Hill Education. 2011.
 15. Ghaednia H, Cermik O, Marghitu DB. Experimental and theoretical analysis of the elasto-plastic oblique impact of a rod with a flat. *Int. J Impact Eng.* 2015; 86:307-17.
 16. Ghaednia H, Cermik O, Marghitu DB. Experimental and theoretical study of the oblique impact of a tennis ball with a racket. *Proc Inst Mech Eng P: J Sport Eng Technol.* 2015;229(3):149-58.
 17. Rothbart HA. *Cam design handbook*. McGraw-Hill Education, USA. 2004.
 18. Angeles J, López-Cajún CS. *Optimization of cam mechanisms*. Springer Science & Business Media, UK. 2012;6.